

Article

Failure Mechanism of Thermal Barrier Coatings on Nozzle Guide Vanes Fabricated from Nickel-Based Single-Crystal Superalloy under Gas Thermal Shock Conditions

Yufeng Wang ^{1,2,*}, Qiangang Fu ^{1,*}, Chenxi Yang ² , Hui Peng ³ and Hua Zhang ²¹ School of Materials Science and Engineering, Northwest Polytechnical University, Xi'an 710072, China² AECC Aviation Power Co., Ltd., Xi'an 710003, China; yangcxyoung@126.com (C.Y.); zhanghua3888@163.com (H.Z.)³ Research Institute for Frontier Science, Beihang University, Beijing 100191, China; penghui@buaa.edu.cn

* Correspondence: wyfeng3705@163.com (Y.W.); fuqiangang@nwpu.edu.cn (Q.F.); Tel.: +86-029-86152732 (Y.W.); +86-029-88492642 (Q.F.)

Abstract: The objective of this study was to investigate the early failure behavior of thermal barrier coatings on single-crystal nozzle guide vanes under gas thermal shock conditions. The microstructure and mechanical properties of the thermal barrier coating before and after the gas thermal shock tests were analyzed using scanning electron microscopy (SEM), energy dispersive spectroscopy (EDS), X-ray diffraction (XRD), and microhardness testing. The results indicate the presence of a mixed layer containing Ni, Cr, Al, Zr, and O at the base of the ceramic layer, and reveal failure behavior in the thermal barrier coating. The analysis suggests that the incomplete formation of the thermal growth oxide layer between the ceramic layer and the bonding layer, before the deposition of the YSZ ceramic layer, led to the easy diffusion of elements from the bonding layer into the root of the ceramic layer during the gas thermal shock process, resulting in the formation of a mixed layer. In the test environment, significant thermal stress was generated in the mixed layer, leading to transverse cracks and ultimately causing early failure of the thermal barrier coating. Consequently, the “incomplete initial TGO layer” model is proposed.

Keywords: thermal barrier coating; thermal shock; early failure; mixed layer; TGO

Citation: Wang, Y.; Fu, Q.; Yang, C.; Peng, H.; Zhang, H. Failure Mechanism of Thermal Barrier Coatings on Nozzle Guide Vanes Fabricated from Nickel-Based Single-Crystal Superalloy under Gas Thermal Shock Conditions. *Coatings* **2023**, *13*, 2062. <https://doi.org/10.3390/coatings13122062>

Academic Editor: Cecilia Bartuli

Received: 12 November 2023

Revised: 30 November 2023

Accepted: 5 December 2023

Published: 9 December 2023

Correction Statement: This article has been republished with a minor change. The change does not affect the scientific content of the article and further details are available within the backmatter of the website version of this article.



Copyright: © 2023 by the authors. Licensee MDPI, Basel, Switzerland. This article is an open access article distributed under the terms and conditions of the Creative Commons Attribution (CC BY) license (<https://creativecommons.org/licenses/by/4.0/>).

1. Introduction

Thermal barrier coatings (TBCs) are extensively employed on the crucial hot-end components of aircraft engines to enhance their service temperature and lifespan. During operation, these coatings must withstand the damaging effects of severe environmental conditions, such as high temperatures, pressures, corrosion, alternating cold and hot impacts, and foreign object impacts, leading to various possible failure modes [1–5].

Typically, the thermal barrier coating system consists of an upper yttria-stabilized zirconia (YSZ) ceramic layer and a lower MCrAlY (M: Ni, Co, or Ni + Co) bonding layer [6]. Under the high-temperature service conditions of the engine, the YSZ ceramic layer experiences a phase transformation, accompanied by a volume expansion of approximately 5%, which causes the coating to spall under the influence of cold and hot alternation [7]. Elevated temperatures can also accelerate coating sintering, damage the coating's microstructure, and reduce its insulation performance and strain tolerance [8]. Due to oxidation, a thermally grown oxide (TGO) layer forms between the bonding layer and the ceramic layer. The excessive thickening of the TGO layer can lead to significant internal stress between the bonding layer and the ceramic layer, resulting in coating spallation and failure [9]. The erosion of molten sediments in the environment (such as CaO-MgO-Al₂O₃-SiO₂, abbreviated as CMAS) is also a primary cause of failure for thermal barrier coatings [10,11]. Once CMAS adheres to the thermal barrier coating, it penetrates and reacts with the coating, causing the latter to spall.

The overall performance of a material is primarily determined by its microstructure, which comprises factors such as crystal size, shape, and orientation [12,13]. Commonly employed techniques for the fabrication of thermal barrier coatings encompass electron beam physical vapor deposition and thermal spray technologies, such as atmospheric plasma spraying [14]. Thermal barrier coatings featuring columnar microstructures prepared via electron beam physical vapor deposition exhibit exceptional strain tolerance and effectively suppress crack propagation, thereby significantly prolonging the coating's operational lifespan [15,16]. In the realm of high-temperature thermal protection for aviation engines, electron beam physical vapor deposition has gained widespread application.

In recent years, however, the early failure of EB-PVD-prepared thermal barrier coatings in aero engines, i.e., failure before reaching the end of their designed service life, has been increasingly witnessed in the engineering field. This failure mode, characterized by large-area spallation of the coating following short-term engineering examination, differs from the conventional failure modes mentioned above. Due to the frequent occurrence of this failure mode, it has emerged as one of the "pain points" in the process of engineering application research for thermal barrier coatings. Following the early failure of the thermal barrier coating, local high-temperature ablation of turbine vanes will occur during service, potentially leading to vane fracture and a catastrophic accident. However, replacing vanes without a thermal barrier coating before the end of their designed service life will reduce the engine's service life cycles and increase its maintenance cost.

With the increasing demand for aircraft engines [6], thermal barrier coating technology, as a pivotal core technology in the field of aviation engine technology, is poised to gain a wider application. The ability to address premature failure issues of thermal barrier coatings on aircraft engines is crucial for the advancement and implementation of this technology. Furthermore, with the development of novel aircraft engine types, turbine blade operating temperatures are increasing and, consequently, thermal barrier coatings have become indispensable in ensuring stable turbine blade operation. Henceforth, resolving the issue of early failure in thermal barrier coatings on aircraft engines will be of paramount importance in facilitating the development of new-generation aircraft engines.

In order to investigate the early failure of thermal barrier coatings fabricated using electron beam physical vapor deposition (EB-PVD), this study employs a combination of multi-arc ion plating and EB-PVD techniques to fabricate the thermal barrier coating. The microstructure of the coating after experiencing gas thermal shock is examined, the failure mode of the coating is analyzed, and the underlying failure mechanism is elucidated. Based on this research, an "initial TGO layer incompleteness" model is proposed to explain the premature spallation of the coating, and a solution is provided to address the early failure of EB-PVD thermal barrier coatings. This investigation not only supplements the understanding of failure modes in thermal barrier coatings but also offers theoretical and technical foundations for the successful incorporation of single-crystal superalloys with thermal barrier coatings in aerospace engines. Furthermore, it provides valuable reference insights for the theoretical exploration and engineering implementation of thermal barrier coatings.

2. Materials and Methods

2.1. Material Preparation

In this study, a nickel-based single-crystal superalloy nozzle guide vane was employed as the substrate material for a thermal barrier coating, to accurately represent the coating's state under thermal shock conditions in engineering applications. The nozzle guide vane, composed of airfoil I and airfoil II, is shown in Figure 1. Cooling slots and film cooling holes were incorporated for effective cooling. A NiCrAlYSi bonding layer was deposited on the vane's surface using multi-arc ion plating technology, with key parameters including a deposition temperature of 500 °C, a bias voltage of 100 V, an arc source current of 150 A, and a deposition time of 8 h. The chemical composition of the NiCrAlYSi ingots is given in Table 1; the thickness of the prepared bonding layer was approximately 30 µm.

Subsequently, the substrate with the NiCrAlYSi bonding layer was insulated for 2 h at 980 °C in a vacuum environment to enhance adhesion. A YSZ ceramic layer was then fabricated using electron beam physical vapor deposition (EB-PVD) technology, with specific process parameters including a deposition temperature of 900 °C, a rotational speed of 20 rpm, a voltage of 20 kV, an evaporation current of 1.4 A, and a deposition time of 0.5 h. The chemical composition of the ceramic ingots is displayed in Table 2; the thickness of the ceramic layer was approximately 110 µm. The selection of the aforementioned preparation parameters was based on our experimental research and validated through engineering verification, ensuring the attainment of exceptional coating quality.

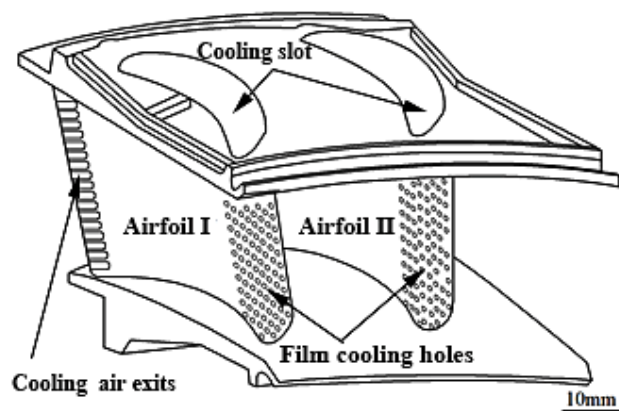


Figure 1. The 3D profile of single-crystal nozzle guide vane.

Table 1. Chemical composition of NiCrAlYSi ingots (wt. %).

Ni	Cr	Al	Y	Si
Bal.	23.5	15.8	1.1	1.3

Table 2. Chemical composition of YSZ ceramic ingots (wt. %).

Y ₂ O ₃	Total Impurities (Si/Mn/Ni/Cr/Fe/V)	ZrO ₂
8.2	≤0.10	Bal.

2.2. Characterization Methods

The thermal shock performance of the as-prepared thermal barrier coating was evaluated in a simulated engine service environment. The testing conditions were as follows: subjecting the vane to a high-temperature gas of 1150 °C for 5 min, followed by a rapid cooling phase of 5 min in a compressed air environment of 0.4~0.5 MPa. The gas mixture consisted of acetylene and oxygen, with a flow rate of 1.2 Ma. During the thermal shock process, the vane was rotated at a speed of 10 rpm, powered by the equipment, to ensure a uniform and consistent impact assessment across the entire vane. The test was repeated until the coating spalled.

The surface and cross-section morphology of the coating was examined, in both the as-prepared state and the after-thermal-shock state, using scanning electron microscopy (SEM, Carl Zeiss SUPRA55, Oberkochen, Germany) with an energy dispersive spectrometer (EDS). The phase composition of the coating was determined using X-ray diffraction (XRD, D/MAX-2500, Rigaku, Tokyo, Japan). To examine the γ' phase morphology of the substrate superalloy, an electrolytic corrosion operation was performed on the vane, using a 3% nital solution. Additionally, the hardness of different layers within the thermal barrier coating was analyzed by employing a Vickers hardness tester (Dura Scan, Struers, Ballerup, Denmark), with a test force of HV 0.5, to measure their respective hardness values.

3. Results

3.1. Microstructure and Phase Composition of the As-Prepared Coating

The cross-section and surface microstructures of the as-prepared thermal barrier coating are presented in Figure 2a,b, respectively. The deposited YSZ ceramic layer exhibits a typical columnar crystal structure, with a crystal size of approximately 5 to 6 μm . The interface between the bonding layer and the ceramic layer is distinct, and no microcracks are visible. Notably, after vacuum thermal diffusion, a thin interdiffusion zone forms at the interface between the substrate and the bonding layer. Elemental composition analysis was conducted on the cross-section region (Figure 2a), with the analysis site evenly divided into 20 test areas (spaced approximately 5 μm apart) from the substrate to the ceramic layer. The elemental contents in each test area were recorded separately, and a graph of the elemental composition trend was generated, as shown in Figure 2c. A limited amount of element interdiffusion behavior can be observed. The interdiffusion zone is attributed to the internal diffusion of the elements Cr and Al from the bonding layer into the substrate, and the external diffusion of Ni, W, and the strengthening elements Mo, Ta, and Re from the substrate into the bonding layer [17,18].

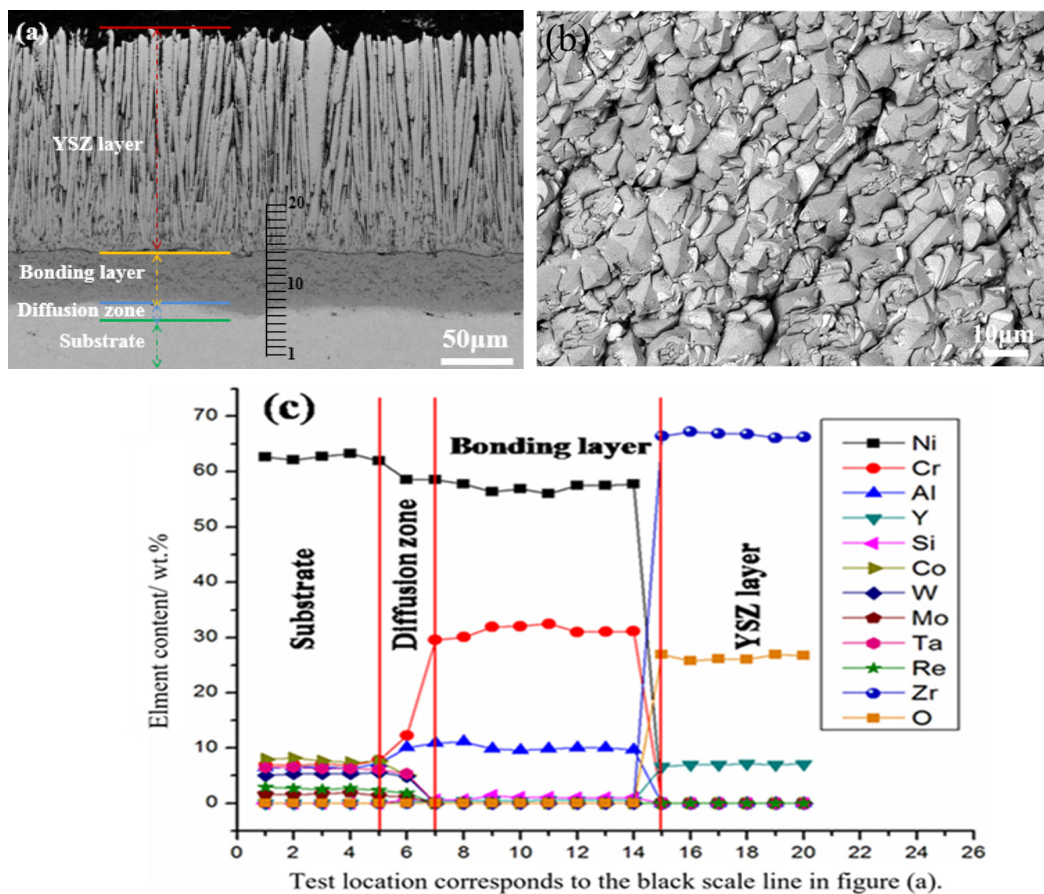


Figure 2. The microstructure and elemental composition trend of the as-prepared thermal barrier coating: (a) cross-section morphology, (b) surface morphology, (c) elemental composition trend.

The phase structure patterns of the as-prepared thermal barrier coating are presented in Figure 3. The primary phase structure of the NiCrAlYSi bonding layer consists of γ' -Ni₃Al and β -NiAl phases (Figure 3a). The dominant phase structure of the YSZ ceramic layer is t' -ZrO₂ (Figure 3b).

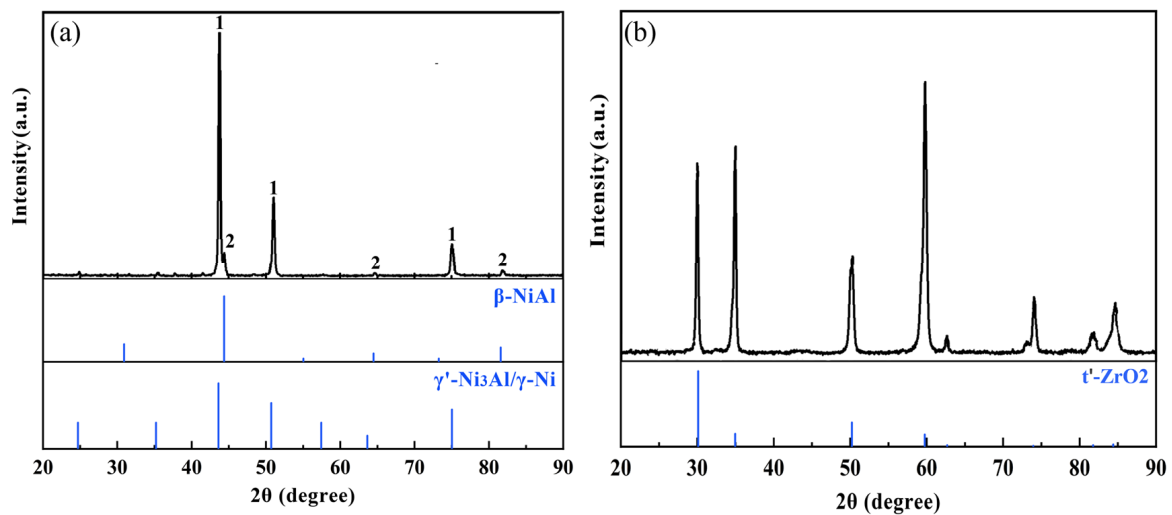


Figure 3. XRD pattern of the NiCrAlYSi bonding layer and the ceramic layer of the as-prepared thermal barrier coating: (a) bonding layer, (b) YSZ ceramic layer.

3.2. Structure Morphology of the Thermal Barrier Coating after Thermal Shock

Figure 4 displays the macroscopic morphology of the nozzle guide vane coated with a thermal barrier coating after 355 gas thermal shock tests. Yellow carbon deposits, generated by gas combustion, are visible in the basin (Figure 4a) and on the back (Figure 4b) of the nozzle guide vane. The residual carbon deposit in the vane basin is greater than that on the back. No spallation of the thermal barrier coating was observed in the vane basin, whereas spallation occurred at similar positions on the back of these two airfoils, exhibiting an irregular long strip shape in the spallation area.

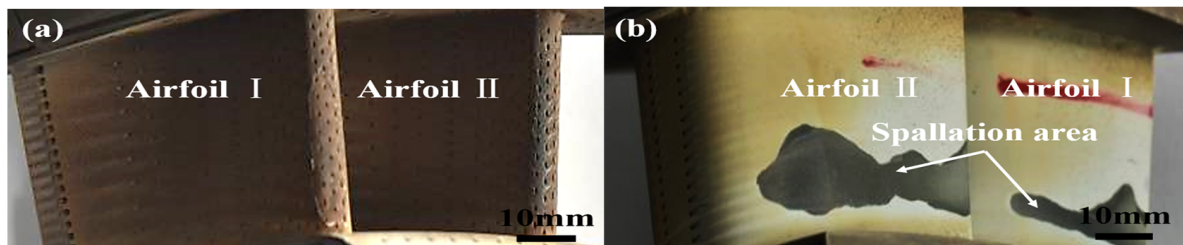


Figure 4. The macro-morphology of the nozzle guide vane after the gas thermal shock test: (a) vane basin; (b) vane back.

The cross-section and surface morphologies of the YSZ ceramic layer at the spallation area from the vane back were analyzed using SEM, as illustrated in Figure 5. The ceramic coatings on airfoil I (presented in Figure 5a,b) and airfoil II (depicted in Figure 5c,d) of the nozzle guide vane exhibit typical columnar crystal structures, characterized by relatively uniform columnar crystal sizes. The transverse average size of columnar crystals is consistent with that of the as-prepared coating, ranging from 5 to 6 μm . This suggests that there is no significant alteration in the size of columnar crystals when compared to the as-prepared coating.

The microstructure of the bonding layer and the ceramic layer at the interface between the coating spalling region and the non-spalling region on the airfoil back was examined, as shown in Figure 6a. Figure 6b presents a local enlarged view of the selected box in Figure 6a. The crack location of the thermal barrier coating is at the base of the ceramic layer, as can be clearly seen. A residual YSZ ceramic layer, approximately 5 μm in thickness, remains on the surface of the bonding layer. Due to the oxidation of Al in the bonding layer, a thin TGO layer is generated between the residual YSZ layer and the bonding layer. Figure 6c illustrates the interface morphology of the coating on the side of the

airfoil basin, and Figure 6d shows the local enlarged view of the selected box in Figure 6c. Although Figure 4a demonstrates that the coating remains intact at the airfoil basin, the microstructure presented in Figure 6d suggests the presence of cracks at the root of the ceramic layer, indicating a slight cracking of the coating. Just as on the back of the airfoil, the presence of TGO can be noted.

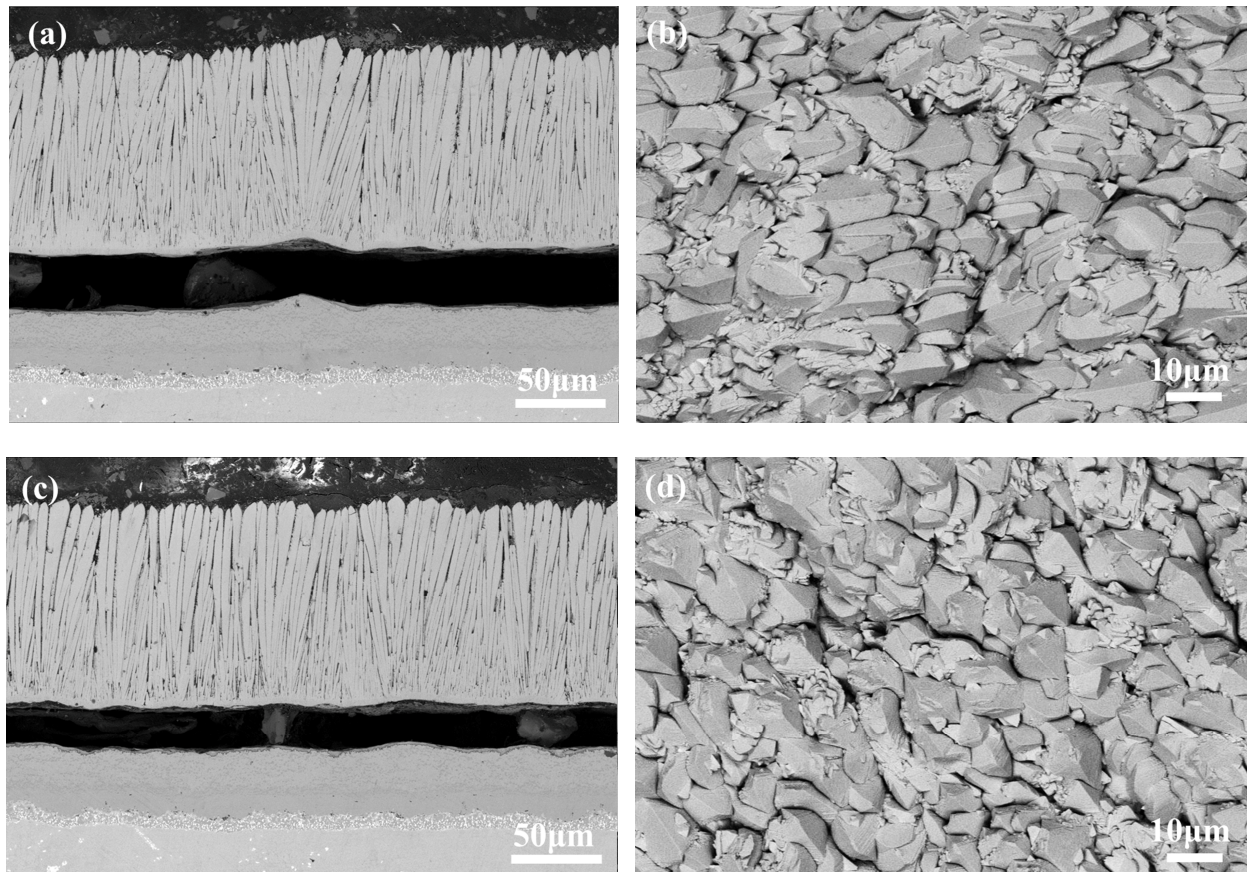


Figure 5. Microstructure of the ceramic coating in the spallation area of the vane back: (a,b) airfoil I; (c,d) airfoil II.

To investigate the distribution of elements within the coating after gas thermal shock, a meticulous point-by-point analysis was performed on the cross-section of the coating (as illustrated in Figure 7a), employing a method analogous to that depicted in Figure 2. This process resulted in the element distribution shown in Figure 7b (See supplementary materials for a mixed map). When examining Figure 7b, it is evident that gas thermal shock produces more significant interdiffusion of elements between the substrate and bonding layers, thereby augmenting the number of precipitated phases as compared to the initial state. Notably, a mixed layer containing elements such as Ni, Cr, and Al is observed between the bonding layer and the ceramic layer, with a thickness of approximately 6–8 μm. In combination with Figure 6, we can infer that the residual YSZ layer in Figure 6 must be part of this mixed layer, and that transverse cracks indeed propagate within the mixed layer. This suggests that the presence of the mixed layer might be the primary cause of the premature coating failure.

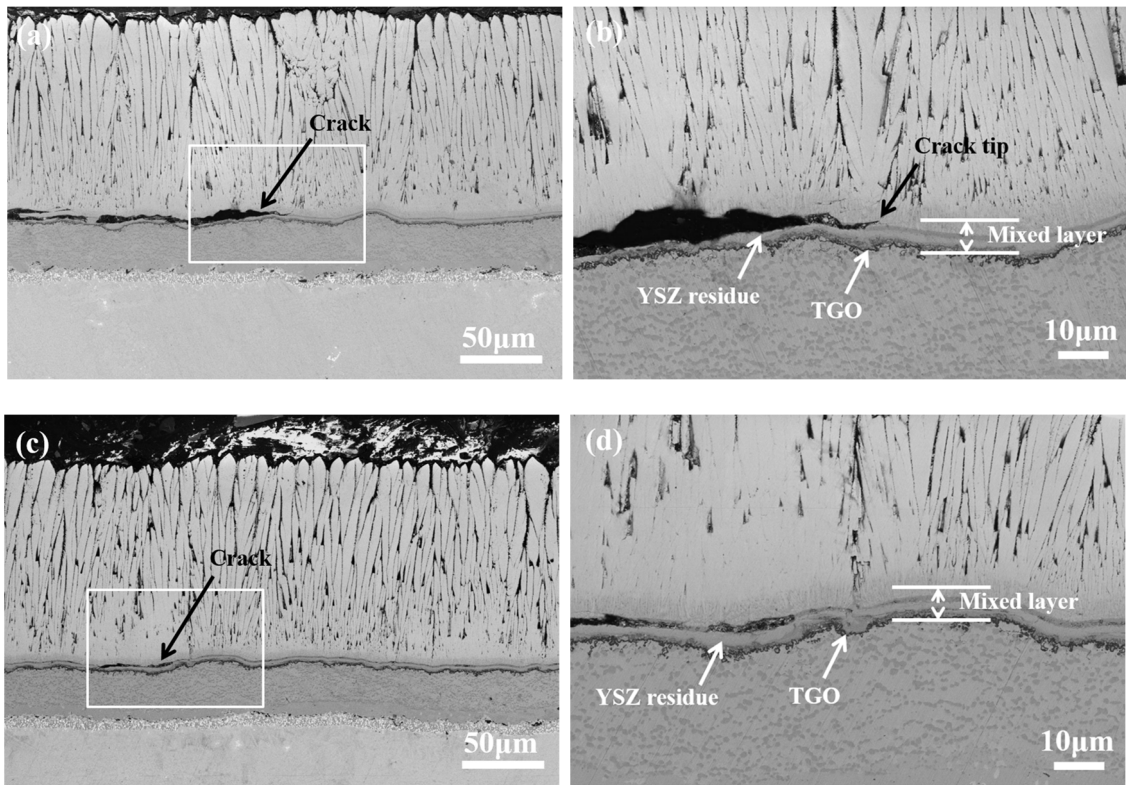


Figure 6. Microstructure of the coating in the spalling and non-spalling zones: (a,b) spalling area of ceramic coating on vane back; (c,d) non-spalling zone of ceramic coating on vane basin.

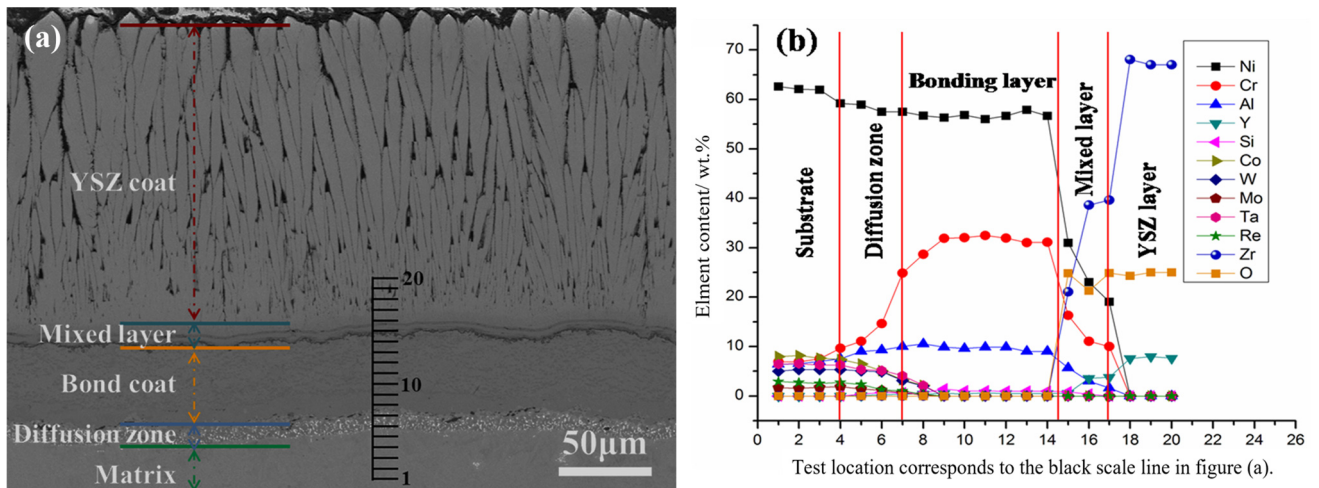


Figure 7. The cross-section microstructure and the elemental composition trend of the coating after gas thermal shock testing: (a) cross-section morphology, (b) elemental composition trend.

3.3. Composition and Microhardness Analysis of the Mixed Layer

In order to conduct a comprehensive analysis of the chemical composition of the mixed layer, EDS analysis was performed on eight distinct regions (as depicted in Figure 8) located within and near the mixed layer. The results are presented in Table 3.

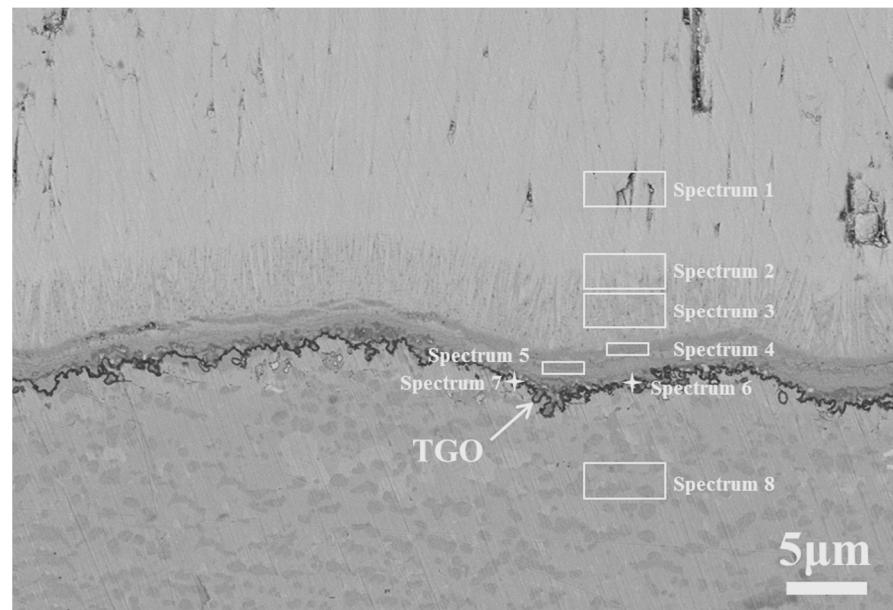


Figure 8. Eight designated regions for the EDS element analysis within and near the mixed layer.

Table 3. EDS results of the different regions in the mixed layer (wt.%).

Spectrum Element	1	2	3	4	5	6	7	8
O	26.9	26.7	22.9	31.8	11.1	35.9	37.7	/
Al	/	1.5	1.3	3.2	8.9	38.0	36.1	10.2
Si	/	/	0.5	3.5	0.6	/	/	0.5
Cr	/	1.4	1.6	27.5	18.3	13.8	5.3	31.3
Ni	/	17.4	56.1	9.9	61.1	5.0	6.5	57.7
Y	6.9	/	2.1	1.7	/	2.0	/	0.3
Zr	66.2	52.9	15.5	22.5	/	5.2	14.5	/

As revealed by Table 3, the mixed layer is primarily composed of the elements Zr, Ni, Cr, and Al. According to the relevant literature, the self-diffusion coefficients of Ni, Cr, and Al in a Ni-Cr-Al ternary alloy are ordered as follows: $D_{Ni} > D_{Al} > D_{Cr}$ [19]. Therefore, it can be clearly seen from spectra 2 and 3 that the element Ni has diffused into this region. Furthermore, due to the high oxygen content, it can be inferred that a substantial amount of NiO spinel phase has been formed. The main elements in spectra 6 and 7 are Al and O, suggesting the initial development of the TGO layer. However, the TGO layer is adulterated with the elements Ni, Cr, and Zr, and the structure exhibits discontinuity.

The microhardness of the metal bonding layer, the mixed layer, and the ceramic layer was analyzed, with five points tested for each layer. The test results are displayed in Table 4. It can be seen in the table that the microhardness values of the mixed layer are higher than those of the bonding layer but lower than those of the ceramic layer, indicating a notable disparity in mechanical properties between the mixed layer and the ceramic layer.

Table 4. Microhardness of the different layers of the thermal barrier coating.

Position	Microhardness/MPa					Average	Standard Deviation
	1	2	3	4	5		
Bonding layer	460	483	479	456	489	473	13.03
Mixed layer	632	619	637	628	633	630	6.11
Ceramic layer	739	728	746	719	734	733	9.24

3.4. Phase Structure Analysis of Substrate and Ceramic Layers

To exclude the possibility of mixed layer formation induced by excessive gas temperature during the gas thermal shock testing process, a comparative analysis of the microstructure of the single-crystal superalloy substrate before and after the thermal shock testing was conducted (Figure 9). After 355 gas thermal shocks at 1150 °C, the γ' phase size of the single-crystal superalloy substrate marginally increased compared to the as-received superalloy, but no γ' phase redissolution occurred. Consequently, we can conclude that no overtemperature phenomenon was present during the test. The growth of the γ' phase under high-temperature conditions represents a normal structural evolution of the substrate during the testing process.

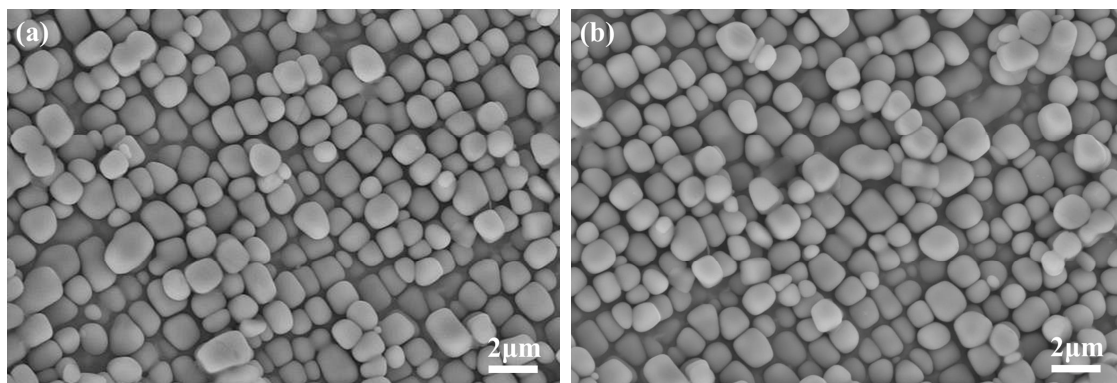


Figure 9. Microstructure of single-crystal alloy before and after thermal shock: (a) before thermal shock, (b) after thermal shock.

Figure 10 shows the XRD result of the YSZ ceramic layer after the thermal shock test. The main phase structure of the YSZ ceramic layer is t' phase, which is unchanged compared to before the test, further indicating that the temperature of the gas thermal shock test does not overtemperature.

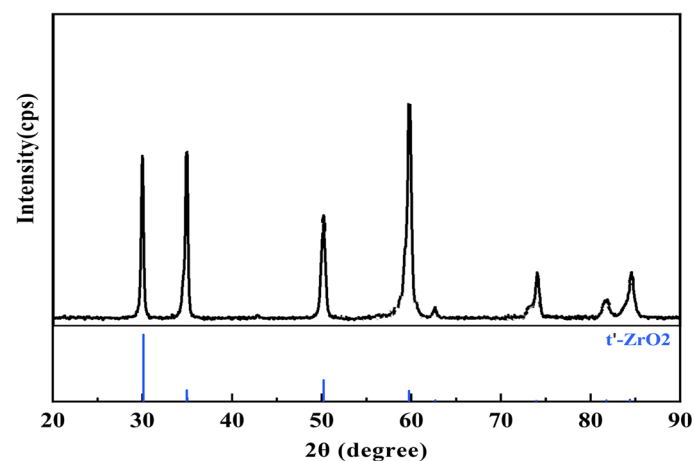


Figure 10. XRD pattern of the YSZ ceramic layer after the thermal shock test.

4. Discussion

The presence of a mixed layer composed of the elements Ni, Cr, Al, Zr, and O, as revealed by the test results from Figures 6–8, is the primary cause of the spallation of the ceramic layer under gas thermal shock test conditions. SEM analysis unambiguously demonstrated the absence of a continuous and intact TGO layer at the interface between the bonding layer and the ceramic layer (Figures 6 and 8), which is consistent with the discontinuity of the TGO layer attributed to the depletion of Al content over an extended

oxidation period [20,21]. Typically, when subjected to long-term oxidation, a TGO layer thicker than 7 μm can generate excessive internal stress, potentially leading to TBC cracking in the TGO layer [22]. Furthermore, the thickening of the TGO layer results in insufficient Al content in the bonding layer, causing the diffusion and oxidation of Ni, Cr, and other elements to form a brittle spinel phase [23]. The gradual thinning of the TGO film eventually leads to the replacement by a spinel phase containing Ni, Cr, Al, Co, and other elements, thereby allowing the spalling of the TBC.

The findings of this study, as illustrated in Figure 7, demonstrate that there was no significant alteration in the Al content within the bonding layer before and after thermal shock. This suggests that the bonding layer does not exhibit Al depletion behavior. In conjunction with Figure 8, the TGO layer remains exceedingly thin subsequent to the thermal shock, with a thickness of less than 1 μm . This thickness is insufficient to cause the TBC failure, according to the aforementioned theory. Thus, the failure mechanism of the TBC in this research cannot be reasonably attributed to Al depletion and TGO thickening.

The current state of the art in the engineering manufacturing process for thermal barrier coatings involves subjecting the bonding layer to vacuum heat treatment, a well-established technique designed to enhance the interfacial bonding between the bonding layer and the substrate [24,25]. This process is characterized by the presence of a β -NiAl phase, which results in the formation of a thin TGO layer on the surface of the bonding layer. This layer, in turn, facilitates the subsequent bonding between the yttria-stabilized zirconia (YSZ) ceramic layer and the bonding layer. However, during the engineering manufacturing process, factors such as blade turnover and inspection must be taken into account. Typically, prior to the ceramic surface preparation, the blade surface requires wet sandblasting and ultrasonic cleaning to achieve the purification of the blade surface, a technique that is extensively employed in the production of thermal barrier coatings. Subsequent to wet sandblasting and ultrasonic cleaning, the TGO layer on the surface of the metal bonding layer is effectively cleaned. The absence of a prefabricated TGO layer in thermal barrier coatings can lead to failure, as demonstrated in this article. This failure mode has been thoroughly verified in engineering manufacturing.

Based on the above experimental findings and analysis, and drawing upon practical experience in engineering manufacturing, we propose the “initial TGO layer incompleteness” model to elucidate the early failure mechanism of thermal barrier coatings.

Figure 11 depicts the “initial TGO layer incompleteness” model. Based on this model, the early failure mechanism of thermal barrier coatings can be summarized as follows: the absence of pre-oxidation in the bonding layer impedes the formation of a complete TGO layer on its surface prior to the initial deposition stage of the ceramic layer, resulting in an incomplete initial TGO layer (Figure 11a). When subjected to a gas thermal shock test, the elements in the bonding layer will diffuse into the root of the ceramic layer in the absence of a complete TGO layer (Figure 11b). As the test duration increases, the elements in the bonding layer further diffuse into the root of the ceramic layer, generating a mixed layer containing elements from both the bonding layer and the ceramic layer (Figure 11c). Given that the mixed layer is composed of multiple phases, such as alumina and nickel oxide, the thermal stress at the interface of these phases can lead to the initiation and propagation of transverse cracks (Figure 11d), ultimately leading to the spallation of the thermal barrier coating.

Based on the theory of the “initial TGO layer incompleteness” model mentioned above, it is imperative to administer a sufficient pre-oxidation treatment to the surface of the bonding layer to achieve a complete TGO layer prior to the fabrication of the ceramic layer. This process can prevent the emergence of a mixed layer, ultimately enhancing the service life and reliability of thermal barrier coatings in engineering applications.

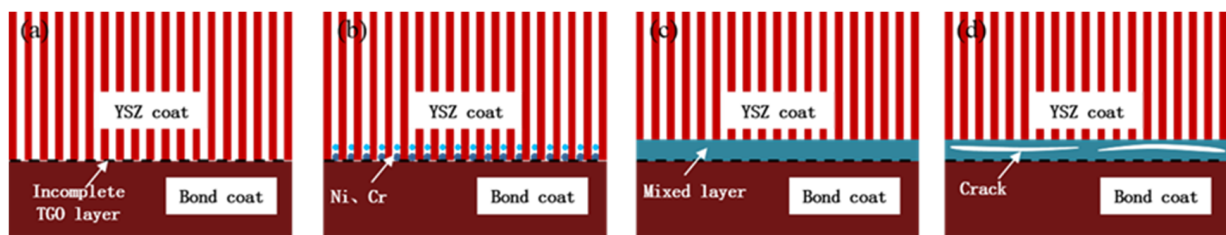


Figure 11. The evolution diagram of the “initial TGO layer incompleteness” model: (a) incomplete TGO layer, (b) element diffusion of the bonding layer, (c) formation of the mixed layer, (d) crack initiation inside the mixed layer.

5. Conclusions

(1) Following 355 iterations of short-term gas thermal shock testing, delamination was observed in the thermal barrier coating. A mixed layer with a thickness of approximately 6–8 μm , consisting of elements such as Ni, Cr, Al, Zr, and O, formed at the interface between the ceramic layer and the bond coat. The microhardness value of this mixed layer was found to be higher than that of the bond coat but lower than that of the ceramic layer.

(2) In accordance with the proposed “initial TGO layer incompleteness” model, the absence of a complete thermally grown oxide (TGO) layer, before the deposition of the YSZ ceramic layer, facilitates the diffusion of elements from the bonding layer to the root of the ceramic layer during the gas thermal shock process, resulting in the formation of a mixed layer. The variation in the thermal expansion coefficient between the various phases within the mixed layer fosters the development of thermal stress, which ultimately leads to the failure of the thermal barrier coating.

(3) Based on the analysis of the “initial TGO layer incompleteness” model, it is crucial to conduct an adequate pre-oxidation treatment on the surface of the bonding layer to form an intact TGO layer before the preparation of the ceramic layer, thereby enhancing the service life and reliability of thermal barrier coatings in engineering applications.

Supplementary Materials: The following supporting information can be downloaded at: <https://www.mdpi.com/article/10.3390/coatings13122062/s1>, Figure S1: The mixed map by overlaying elemental composition trend on the cross-section microstructure image of the coating before and after gas thermal shock testing. (a) before gas thermal shock testing; (b) after gas thermal shock testing.

Author Contributions: Formal analysis, Y.W.; investigation, C.Y.; interpretation of data for the work, Y.W. and Q.F.; writing—original draft preparation, Y.W.; writing—review and editing, C.Y. and H.P.; project administration, H.Z. All authors have read and agreed to the published version of the manuscript.

Funding: This research received no external funding.

Institutional Review Board Statement: Not applicable.

Informed Consent Statement: Not applicable.

Data Availability Statement: Data are contained within the article.

Acknowledgments: The authors thank the anonymous reviewers for their critical and constructive reviews of the manuscript.

Conflicts of Interest: Yufeng Wang, Chenxi Yang and Hua Zhang were employed by AECC Aviation Power Co., Ltd., The remaining authors declare that the research was conducted in the absence of any commercial or financial relationships that could be construed as a potential conflict of interest.

References

- Zhen, Z.; Qu, C.; Fu, D.H. Characterization of the internal stress evolution of an EB-PVD thermal barrier coating during a long-term thermal cycling. *Materials* **2023**, *16*, 2910. [CrossRef] [PubMed]
- Ding, K.; Zhang, T.; Wang, Z.; Yu, J.; Guo, W.; Yang, Y. Effect of thermal growth oxide composition and morphology on local stresses in thermal barrier coatings. *Materials* **2023**, *15*, 8442. [CrossRef] [PubMed]

3. Fan, Z.; Wang, K.; Dong, X.; Wang, R.; Duan, W.; Mei, X.; Wang, W.; Cui, J.; Zhang, S.; Xu, C. The role of the surface morphology and segmented cracks on the damage forms of laser re-melted thermal barrier coatings in presence of a molten salt ($\text{Na}_2\text{SO}_4 + \text{V}_2\text{O}_5$). *Corros. Sci.* **2017**, *115*, 56–67. [[CrossRef](#)]
4. Wu, J.; Gao, Y.; Guo, C.; Guo, L. Laser surface modification to improve the resistance of CMAS + molten salt coupling corrosion to thermal barrier coatings. *Ceram. Int.* **2023**, *49*, 32283–32291. [[CrossRef](#)]
5. Huang, S.; Huang, M.M.; Lyu, Y.J. Seismic performance analysis of a wind turbine with a monopile foundation affected by sea ice based on a simple numerical method. *Eng. Appl. Comp. Fluid.* **2021**, *15*, 1113–1333. [[CrossRef](#)]
6. Bakan, E.; Vaßen, R. Ceramic top coats of plasma-sprayed thermal barrier coatings: Materials, processes, and properties. *J. Therm. Spray. Tech.* **2017**, *26*, 992–1010. [[CrossRef](#)]
7. Moon, J.; Choi, H.; Kim, H.; Lee, C. The effects of heat treatment on the phase transformation behavior of plasma-sprayed stabilized ZrO_2 coating. *Surf. Coat. Tech.* **2002**, *155*, 1–10. [[CrossRef](#)]
8. Lv, B.; Fan, X.; Xie, H.; Wang, T.J. Effect of neck formation on the sintering of air-plasma-sprayed thermal barrier coating system. *J. Eur. Ceram. Soc.* **2017**, *37*, 811–821. [[CrossRef](#)]
9. Torkashvand, K.; Poursaeidi, E.; Mohammadi, M. Effect of TGO thickness on the thermal barrier coatings life under thermal shock and thermal cycle loading. *Ceram. Int.* **2018**, *44*, 9283–9293. [[CrossRef](#)]
10. Peng, H.; Wang, L.; Guo, L.; Miao, W.; Guo, H.; Gong, S. Degradation of EB-PVD thermal barrier coatings caused by CMAS deposits. *Prog. Nat. Sci.* **2012**, *22*, 461–467. [[CrossRef](#)]
11. Iqbal, A.; Moskal, G. Recent development in advance ceramic materials and understanding the mechanisms of thermal barrier coatings degradation. *Arch. Comput. Method. Eng.* **2023**, *30*, 4855–4896. [[CrossRef](#)]
12. Tian, X.; Zhao, Y.; Gu, T.; Guo, Y.; Xu, F.; Hou, H. Cooperative effect of strength and ductility processed by thermomechanical treatment for Cu–Al–Ni alloy. *Mater. Sci. Eng. A.* **2022**, *849*, 143485–143495. [[CrossRef](#)]
13. Zhu, Q.; Chen, J.; Gou, G.; Chen, H.; Li, P. Ameliorated Longitudinal Critically Refracted -Attenuation Velocity Method for Welding Residual Stress Measurement. *J. Mater. Process Technol.* **2017**, *246*, 267–275. [[CrossRef](#)]
14. Vaßen, R.; Mack, D.E.; Tandler, M.; Sohn, Y.J.; Sebold, D.; Guillon, O. Unique performance of thermal barrier coatings made of yttria-stabilized zirconia at extreme temperatures ($>1500\text{ }^\circ\text{C}$). *J. Am. Ceram. Soc.* **2021**, *104*, 463–471. [[CrossRef](#)]
15. Toriz, F.C.; Thakker, A.B.; Gupta, S.K. Flight service evaluation of thermal barrier coatings by physical vapour deposition at 5200h. *Surf. Coat. Technol.* **1989**, *39–40*, 161–172. [[CrossRef](#)]
16. Wellman, R.G.; Nicholls, J.R. A mechanism for the erosion of EB-PVD TBCs. *Mater. Sci. Forum.* **2001**, *369–372*, 531–538. [[CrossRef](#)]
17. Wu, Y.; Wang, Y.M.; Song, G.M.; Li, X.W. The Improvement of oxidation resistance of a Re-based diffusion barrier/Ni–Al coating on the single-crystal Ni-based TMS-82+ superalloy. *Oxid. Met.* **2011**, *76*, 419–431. [[CrossRef](#)]
18. Pillai, R.; Sloof, W.G.; Chyrkin, A. A new computational approach for modelling the microstructural evolution and residual lifetime assessment of MCrAlY coatings. *Mater. High. Temp.* **2015**, *32*, 57–67. [[CrossRef](#)]
19. Yu, S.; Wang, C.Y.; Yu, T.; Cai, J. Self-diffusion in the intermetallic compounds NiAl and Ni_3Al -An embedded atom method study. *Phys. B* **2007**, *396*, 138–144. [[CrossRef](#)]
20. Shillington, E.A.G.; Clarke, D.R. Spalling failure of a thermal barrier coating associated with aluminum depletion in the bond-coat. *Acta. Mater.* **1999**, *47*, 1297–1305. [[CrossRef](#)]
21. Che, C.; Wu, G.Q.; Qi, H.Y.; Huang, Z.; Yang, X.G. Depletion model of aluminum in bond coat for plasma-sprayed thermal barrier coatings. *Adv. Mat. Res.* **2009**, *75*, 31–35. [[CrossRef](#)]
22. Shen, Q.; Yang, L.; Zhou, Y.C.; Wei, Y.G.; Zhu, W. Effects of growth stress in finite-deformation thermally grown oxide on failure mechanism of thermal barrier coatings. *Mech. Mater.* **2017**, *114*, 228–242. [[CrossRef](#)]
23. Shamsipoor, A.; Farvizi, M.; Razavi, M.; Keyvani, A.; Mousavi, B.; Pan, W. High-temperature oxidation behavior in YSZ coated Cr_2AlC and CoNiCrAlY substrates. *Surf. Coat. Tech.* **2020**, *401*, 126239–126248. [[CrossRef](#)]
24. Karaoglanli, A.C.; Dikici, H.; Kucuk, Y. Effects of heat treatment on adhesion strength of thermal barrier coating systems. *Eng. Fail. Anal.* **2013**, *32*, 16–22. [[CrossRef](#)]
25. Rätzer-Scheibe, H.J.; Schulz, U. The effects of heat treatment and gas atmosphere on the thermal conductivity of APS and EB-PVD PYSZ thermal barrier coatings. *Surf. Coat. Tech.* **2007**, *201*, 7880–7888. [[CrossRef](#)]

Disclaimer/Publisher’s Note: The statements, opinions and data contained in all publications are solely those of the individual author(s) and contributor(s) and not of MDPI and/or the editor(s). MDPI and/or the editor(s) disclaim responsibility for any injury to people or property resulting from any ideas, methods, instructions or products referred to in the content.